We are IntechOpen,
the world's leading publisher of
Open Access books
Built by scientists, for scientists

4,800
Open access books available

122,000
International authors and editors

135M
Downloads

Our authors are among the

154
Countries delivered to

TOP 1%
most cited scientists

12.2%
Contributors from top 500 universities

BOOK CITATION INDEX
CLARIVATE ANALYTICS
INDEXED

WEB OF SCIENCE™

Selection of our books indexed in the Book Citation Index
in Web of Science™ Core Collection (BKCI)

Interested in publishing with us?
Contact book.department@intechopen.com

Numbers displayed above are based on latest data collected.
For more information visit www.intechopen.com

Effect of Polymorphism on the Particle and Compaction Properties of Microcrystalline Cellulose

John Rojas

Additional information is available at the end of the chapter

http://dx.doi.org/10.5772/56591

1. Introduction

Cellulose is the most abundant natural linear polymer. It consists of 1,4-linked-β-D-glucose units and is known to exist in the following distinct allomorphs: I_α (from algae and bacteria), I_β (from superior plants), II (the most stable form produced by mercerization), III_I and III_{II} (prepared from ammonia at -30 ºC), and IV_I and IV_{II} (produced at 260 ºC in glycerol). Each allomorph differs in its physicochemical properties [1,2]. Cellulose III is formed when native cellulose is treated with liquid ammonia at low temperatures, whereas cellulose IV is obtained by treatment of regenerated cellulose at high temperatures (Figure 1) [3]. However, the last two forms have no pharmaceutical applications.

Of these, the cellulose I (MCCI) allomorph is the most prevalent form and cellulose II is the most stable form [4]. MCCI can be converted to MCCII, but not vice versa [5,6]. As shown in Figure 2, in cellulose I (MCCI), the chain orientation is exclusively parallel [3], whereas in cellulose II (MCCII) the chains are arranged in an anti-parallel orientation.

Commercial microcrystalline cellulose (MCCI) contains the cellulose I lattice. It is obtained from wood pulp by treatment with dilute strong mineral acids (HCl, H_2SO_4, HNO_3) at boiling temperatures until the degree of polymerization levels-off [7,8]. The acid hydrolyzes the less ordered regions of the polymer chains, leaving the crystalline regions intact. This MCCI is also called hydrolyzed cellulose or hydrocellulose.

Since the 1970s, microcrystalline cellulose I (MCCI) has been the dominant excipient used for direct compression due to its good diluent and binding properties and low moisture content. The strong binding properties of MCCI are due to hydrogen bonding among the plastically deforming cellulose particles. However, it suffers from sensitivity to lubricants
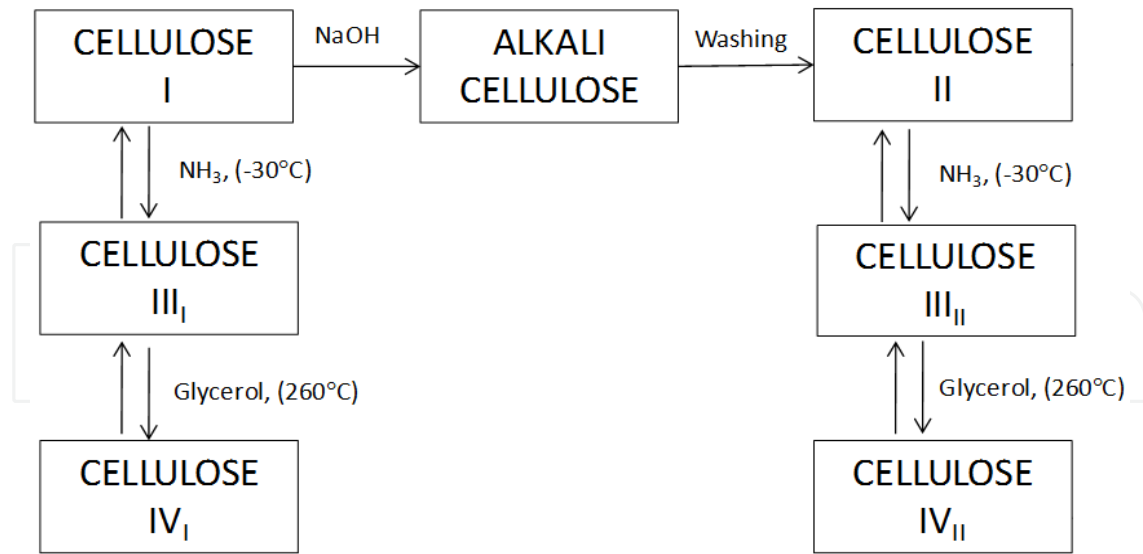
Figure 1. Scheme for the formation of cellulose allomorphs
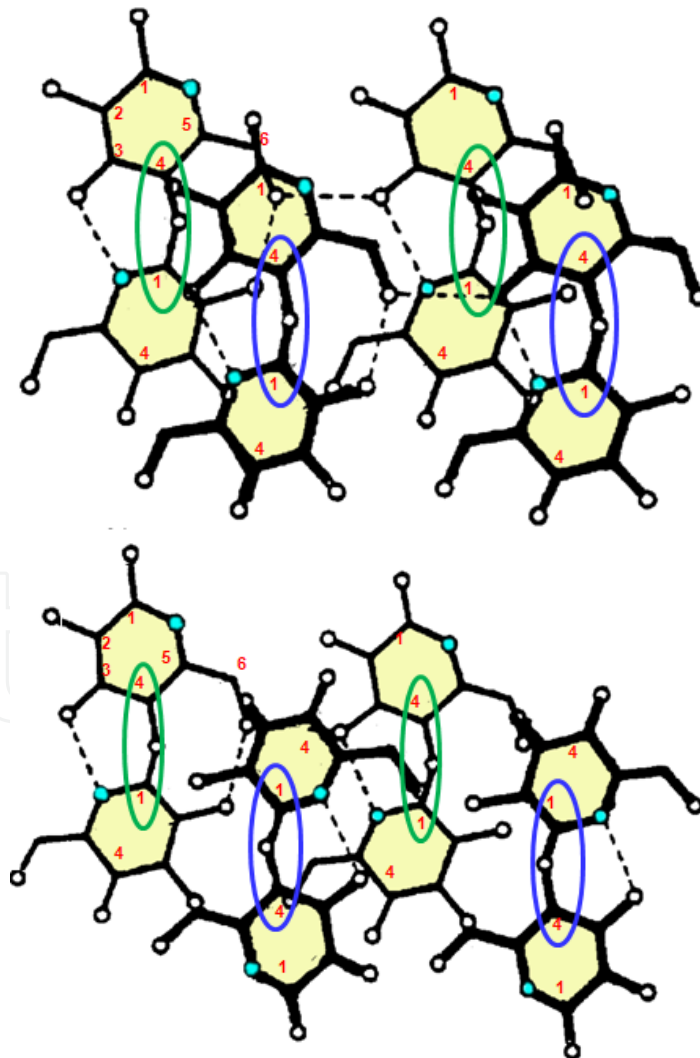
Figure 2. Conformations of MCCI (A) and MCCII (B)

and poor flow [9,10]. Because of its strong binding properties, it requires the addition of a disintegrant for an effective drug release, making formulations more costly. The compactibility of MCCI is also adversely affected when processed by high shear wet granulation since upon drying part of the water interacts with cellulose through hydrogen bonding and as a result, these hydrogen bonds are not available for further particle bonding [11].

Recently, microcrystalline cellulose II (MCCII) was introduced as a new direct compression excipient [12]. It can be produced by soaking MCCI in an aqueous sodium hydroxide solution (> 5 N) at a 1:6 weight-to-volume ratio for 14 h at room temperature, with occasional stirring. The resulting MCCII gel is then precipitated (regenerated) with a 50-60% aqueous ethanolic solution, filtered, washed with distilled water to neutrality by decantation, filtered again, and dried at 40 °C until reaching a moisture content of less than 5 % [13]. During this process, the amorphous regions of the microfibrils are partially eliminated leaving the most crystalline parts intact. The resulting product is usually washed and spray-dried to get a powder [14].

In most cases, a polymorphic transformation could modify some of the particle properties of a material. One of those properties is related to the water uptake capacity of the powder. In fact, this uptake depends on the crystalline structure of the polymer. Further, the mechanical and disintegrating properties of these materials are related to the degree of crystallinity and water uptake capacity, respectively. Thus, knowledge of the water sorption behavior of the cellulose allomorphs is essential to understand and predict their stability, especially during storage, alone or combined with other materials in a dosage form under variable ambient conditions. In this study, the effect of polymorphic transformation on the microcrystalline cellulose functionality was evaluated. The particle and mechanical properties of MCCII were assessed and compared with those of commercial MCCI (Novacel® PH-101).

2. Experimental

2.1. Materials

MCCI (Novacel PH-101, lot 6N608C) was donated by FMC Biopolymers, Philadelphia, PA, USA. Sodium hydroxide (lot 58051305C) and concentrated hydrochloric acid (37%, lot k40039517) were obtained from Carlo Erba, and Merck, respectively. Magnesium stearate (lot 2256KXDS) was purchased from Mallinckrodt Baker and acetaminophen (lot GOH0A01) was obtained from Sigma-Aldrich.

2.2. Methods

2.2.1. Preparation of Microcrystalline Cellulose II (MCCII)

Approximately, 500 g of MCCI was soaked in 3 L of 7.5 N NaOH for 72 h at room temperature. The cellulose II thus obtained was washed with distilled water until it reached neutral pH. The slurry was sequentially passed through 6 (3350 μm), 10 (2000 μm), 24 (711 μm), 40 (425 μm) and 100 (150 μm) mesh screens using an oscillating granulator (Riddhi

Pharma Machinery, Gulabnagar, India) when the moisture content was ~60, 50, 40, 30 and 20%, respectively. The final material was dried in a convection oven at 60°C (Model STM 80, Rigger Scientific Inc, Chicago, IL) to a moisture content of less than 5%.

2.2.2. Fourier-Transform Infrared Spectroscopy (FT-IR) Characterization

Approximately, 1.5 mg of sample was mixed with about 300 mg of dry potassium bromide (previously dried at 110 °C for 4 h) with an agate mortar and pestle. The powdered sample was compressed into a pellet using a 13 mm flat-faced punch a die tooling fitted on a portable press at a dwell time of five minutes. A Perkin Elmer spectrophotometer (Spectrum BX, Perkin Elmer, CA, USA) equipped with the Spectrum software (Perkin Elmer, Inc, CA, USA) was used to obtain the spectrum between 650 to 4000 cm^{-1}. The resolution, interval length and number of scans employed were 16, 2.0 and 16 cm^{-1}, respectively.

2.2.3. Powder X-Rays (P-XRD) Characterization

Powder X-ray diffraction (P-XRD) measurements were conducted over a 5 to 45º 2θ range using a Rigaku Bench top, diffractometer (Miniflex II, Rigaku Americas, The Woodlands, TX, USA) at 40 kV and 30 mA equipped with monochromatic CuK$_\alpha$ (α_1=1.5460 Å, α_2= 1.54438 Å) X-ray radiation. The sweep speed and step width were 0.5º 2θ/min and 0.008°, respectively. The PeakFit software, version 4.12 (SeaSolve Inc, Framingham, MA) was used for the calculation of the areas. The degree of crystallinity was found from the equation [15]:

$$DC = \frac{I_C}{I_T} * 100\% \qquad (1)$$

Where I$_C$ is the sum of the areas of all crystalline peaks and I$_T$ is the area of the amorphous and crystalline regions.

2.3. Powder properties

The microphotographs were taken on an optical microscope (BM-180, Boeco, Germany) coupled with a digital camera (S8000fd, Fujifilm Corp., Japan) at 700X magnification. The true density was determined on a helium picnometer (AccuPyc II 1340, Micromeritics, USA) with ~2 g of sample. Bulk density was determined by the ratio of 20 g of sample divided the measured volume. Tap density was measured directly from the final volume of the tapped sample obtained from the AUTO-TAP analyzer (AT-2, Quantachrome instruments, USA). Flow rate was obtained by measuring the time for ~20 g of sample to pass through a glass funnel (13 mm diam). Porosity (ε) of the powder was determined from the equation:

$$\varepsilon = 1 - \left(\frac{\rho_{bulk}}{\rho_{true}}\right) \qquad (2)$$

Where, ε, ρ$_{bulk}$, and ρ$_{true}$ are the porosity, bulk density and true density of the powder, respectively. The degree of polymerization (DP) was obtained by the intrinsic viscosity

method [η] at 25 ±0.5 °C using a Canon-Fenske capillary viscometer (cell size 50) and cupriethylendiamine hydroxide (CUEN) as solvent [16]. The DP was found by the relationship:

$$DP = 190 * [\eta] \qquad (3)$$

The compressibility of the powder was obtained by applying the Kawakita model [17]:

$$N / \left[(V_i - V_n) / V_i \right] = N / a + 1 / ab \qquad (4)$$

Where, N is the tap number, V_i the initial volume and V_n the volume at the respective tap number. The constant "a" is related to the total volume reduction for the powder bed (compressibility index) and the constant "b" is related to the resistant forces (friction/cohesion) to compression [18].

2.4. Particle size

Samples were fractionated on a RO-TAP sieve shaker (RX29, W.S. Tyler Co., Mentor, OH, USA) using stainless steel 420, 250, 180, 125, 105, 75 μm sieves, stacked together in that order (Fisher Scientific Co., Pittsburgh, PA, USA). Approximately, 50 g of the sample was shaken for 30 min followed by weighing the fractions retained in each sieve. The particle size distributions and the geometric means were found from the log-Normal distributions using the Minitab software (v.16, Minitab®, Inc., State College, PA).

2.5. Swelling studies

The swelling value is expressed as the ratio of the expanded volume of the powder upon water addition and the initial sample weight. Approximately, 500 mg of the powder was vigorously dispersed in a 10 ml graduate cylinder filled with 10 ml of distilled water at room temperature and the increase in volume of the powder was measured with time [19].

2.6. Water sorption isotherms

Water sorption isotherms were conducted on a VTI Symmetric Gravimetric Analyzer (Model SGA-100, VTI Corporation, Hialeah, FL), equipped with a chilled mirror dew point analyzer (Model Dewprime IF, Edgetecth ford, MA) at 25 °C. The water activity employed ranged from 0 to 0.9. Water uptake was considered at equilibrium when a sample weight change of no more than 0.01% was reached. Samples were analyzed in triplicate. The non-linear curve fitting and the resulting parameters were obtained using the Statgraphic software vs. 5 (Warrenton, VA). The Young-Nelson Model (YN) was used for data fitting. This model distinguishes between the tightly bound monolayer, normally condensed externally adsorbed water, and internally absorbed water [20]. In this model, water uptake is given by equations 5-9:

$$m = A(\theta + \beta) + B\Psi \qquad (5)$$

$$\theta = \frac{a_w}{a_w + (1 - a_w)E} \tag{6}$$

$$\Psi = a_w \theta \tag{7}$$

$$\beta = -\frac{Ea_w}{E - (E-1)a_w} + \left(\frac{E^2}{E-1}\right)\ln\frac{E - (E-1)a_w}{E} - (E+1)\ln(1 - a_w) \tag{8}$$

$$E = e^{-(H1 - Hl)/RT} \tag{9}$$

Where, m, θ, Ψ, and B correspond to the total fractional moisture content, the fraction of molecules cover by monolayer, the fraction covered by a layer 2 or more molecules thick, and the amount of absorbed water in the multilayer. H_1 is the heat of adsorption of water bound to the surface, H_L the heat of condensation, R is the gas constant (8.31 J/Kmol), and T the temperature. A and B are dimensionless constants related to the fraction of adsorbed and absorbed water on the polymer, respectively. E is the equilibrium constant between the monolayer and liquid water. The product Aθ is related to the amount of water in the monolayer and A(θ+B) is the externally adsorbed moisture during the sorption phase. BΨ is the amount of moisture absorbed during the sorption phase [21].

2.7. Tableting properties

Compacts of ~500 mg each were made on a single punch tablet press (Compac 060804, Indemec Ltd, Itagui, Colombia) coupled with a load cell (Model LCGD-10K, Omega Engineering, Inc., Stamford, CT) using flat-faced 13 mm punches and die tooling for 1 and 30 s. Pressures ranged from ~35 to ~190 MPa. Forces were measured on a strain gauge meter (Model DPiS8-EI, Omega Engineering, Inc., Stamford, CT). Compact heights were measured immediately after production and after 5 days of storage to measure the elastic recovery of the material.

2.8. Compressibility analysis

The natural logarithm of the inverse of compact porosity, $[-\ln(\varepsilon)]$, was plotted against compression pressure (P) to construct the Heckel plot [22, 23]. The slope (m) of the linear region of this curve is inversely related to the material yield pressure (P_y), which is a measurement of its plasticity [24]. Thus, a low P_y (usually values <100 MPa) indicates a high ductile deformation mechanism upon compression. The Heckel model is given by:

$$-\ln \varepsilon = mP + A \tag{11}$$

Where, A is the intercept obtained by extrapolating the linear region to zero pressure. Other parameters useful in assessing compressibility are D_0, D_a, and D_b, which are related to initial powder packing/densification, total compact densification, and particle rearrangement/fragmentation at the initial compaction stage, respectively [25]. D_0 was

calculated by dividing the bulk density with the true density [26]. The strain rate sensitivity (SRS) was found by the percentage change of the P_y resulted from 1 and 0.03 compact/s speeds, respectively.

2.9. Compact tensile strength

It was determined on a VanKel hardness tester (UK 200, VanKel, Manasquan, NJ, USA). Each compact was placed between the platens and the crushing force was then measured. The radial tensile strength (TS) values were obtained according to the Fell and Newton equation [27]:

$$TS = \frac{2\sigma}{\pi DH} \qquad (12)$$

Where, F is the crushing force (N) needed to break the compact into two halves, D is the diameter of the compact (mm), and t is the compact thickness (mm). The crosshead speed of the left moving platen was 3.5 mm/s.

2.10. Dilution potential

Tablets containing different levels of acetaminophen (25, 50, 75, 85 or 95%) and a poorly compressible drug, were prepared and their crushing strength was determined. Acetaminophen and the test excipient were mixed in a V-Blender for 30 min and then compressed on a single punch tablet press at 120 MPa and a dwell time of 30 s. Samples were analyzed in triplicate.

2.11. Lubricant Sensitivity (LSR)

Lubricant sensitivity was assessed by mixing powders with magnesium stearate at the 99:1 weight ratio in a V-blender (Riddhi Pharma Machinery, Gulabnagar, India) for 30 min. Tablets were prepared using a single punch tablet press at 120 MPa and a dwell time of 30 s. The lubricant sensitivity was expressed as the lubricant sensitivity ratio (LSR) according to the equation:

$$LSR = \frac{H_0 - H_{lub}}{H_0} \qquad (13)$$

Where, H_0 and H_{lub} are the crushing strengths of tablets prepared without and with lubricant, respectively. Samples were analyzed in triplicate.

2.12. Compact friability

The friability test was performed on a friabilator (FAB-25, Logan Instruments Corp., NJ, USA) at 25 rpm for 4 min. An amount of ~6.5 g of compacts made at 150 MPa, each weighing ~500 mg, was tested in a friabilator. Compacts were then dusted and reweighed. The percentage weight loss was taken as friability.

2.13. Compact disintegration

Tablets, each weighing ~500 mg, were made on a single punch tablet press (060804, Indumec, Itagui, Columbia) using a 13 mm round, flat-faced punches and die set. Five replicates were tested in distilled water at 37 °C employing a Hanson disintegrator (39-133-115, Hanson Research Corporation, Northridge, CA, USA) operating at 30 strokes/min.

## 3. Results and discussion

3.1. FT-IR characterization

As seen in Figure 3 the cellulose allomorphs showed no major differences in the infrared bands, except for the vibration peak at 3423 cm^{-1} corresponding to intramolecular OH stretching, including hydrogen bonds and at 2893 cm^{-1} due to CH and CH$_2$ stretching. It is reasonable that these two bands appear displaced due to the rearrangement of the cellulose chains and hydrogen bonding pattern, which is parallel and antiparallel for MCCI and MCCII, respectively. Other main vibrational peaks with virtually no change due to the polymorphic transformation are: 1642 cm^{-1} corresponding to OH from absorbed water, 1427 cm^{-1} due to CH$_2$ symmetric bending, 1375 cm^{-1} due to CH bending, 1330 cm^{-1} due to OH in plane bending, 1255 cm^{-1} corresponding to C-O-H bending, 1161 cm^{-1} due to C-O-C asymmetric stretching (β-glucosidic linkage), 1063 cm^{-1} due to C-O/C-C stretching and 895 cm^{-1} due to the asymmetric (rocking) C-1 (β-glucosidic linkage) out-of-plane stretching vibrations. This band is associated to the cellulose II lattice [28, 29].

3.2. P-XRD characterization

It is well known that the acid hydrolysis of powdered α-cellulose I reduces the degree of polymerization and in turn increases slightly the degree of crystallinity, true density, compact tensile strength and fragmentation tendency [30, 31]. In this study, the change in the above properties is only attributed to the polymorphic form, which is evidenced in the powder x-Rays difractograms (Figure 4). MCCI displayed the characteristic diffraction peaks of the cellulose I lattice at 14.8, 16.3 and 22.4° 2θ, corresponding to the 11$\bar{0}$, 110 and 200 reflections, respectively. A shoulder at 20.4° 2θ has also been also identified in some MCCI excipients [32]. MCCII materials showed crystalline peaks at 12, 20 and 22° 2θ corresponding to the 11$\bar{0}$, 110 and 200 reflections, respectively [2]. The degree of crystallinity of MCCI was larger than that of MCCII. It is plausible that the antiparallel arrangement along with the monoclinic unit cell renders a loose molecular packing and hence causes a lower degree of crystallinity. During the soaking step, the alkali could partially attack the glycosidic bonds located on the less ordered surface of the microfibrils since they are more accessible than the glycosidic bonds located in the ordered regions of the microfibrils of cellulose. This might explain why MCCII has a slightly lower degree of crystallinity than MCCI.
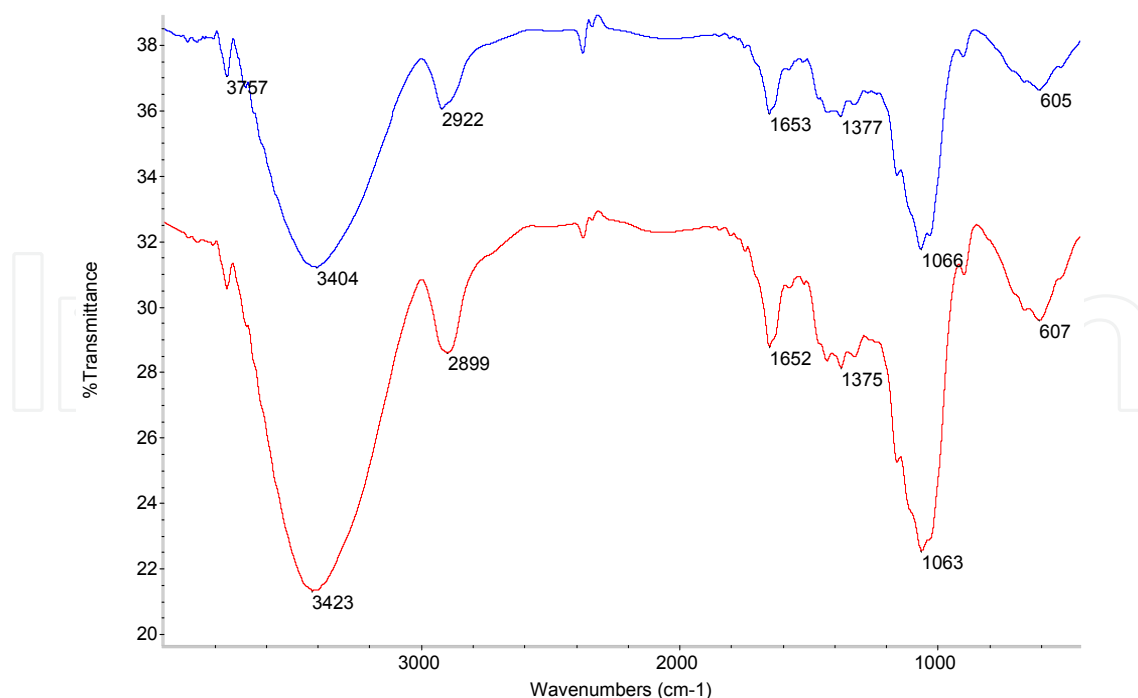
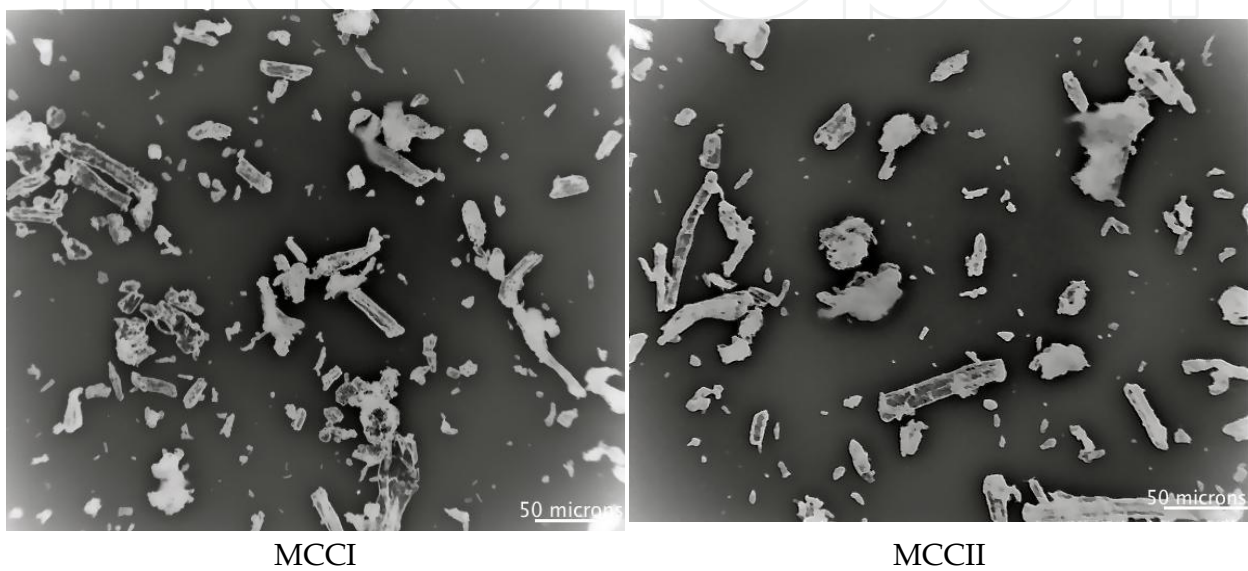**Figure 3.** FT-IR of microcrystalline cellulose allomorphs
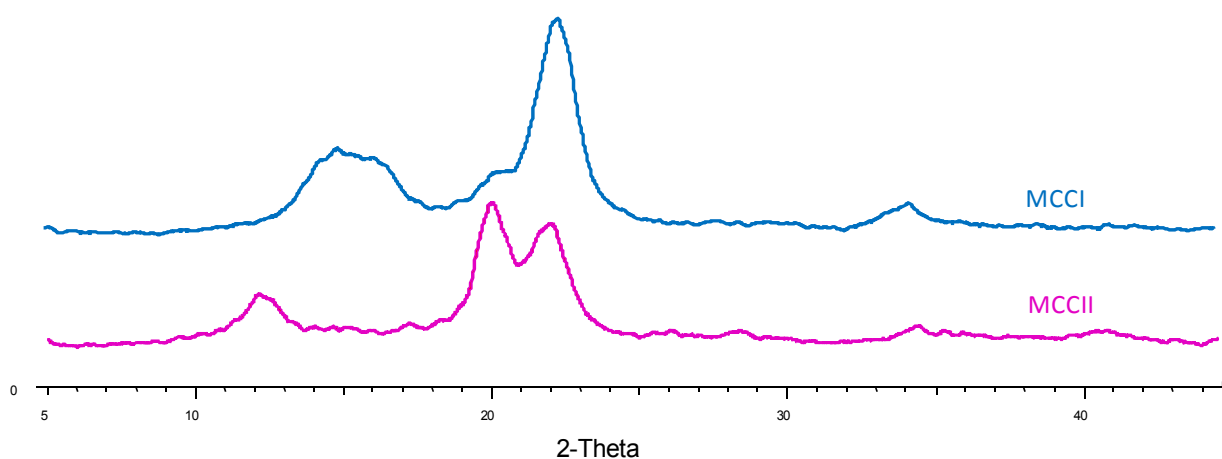
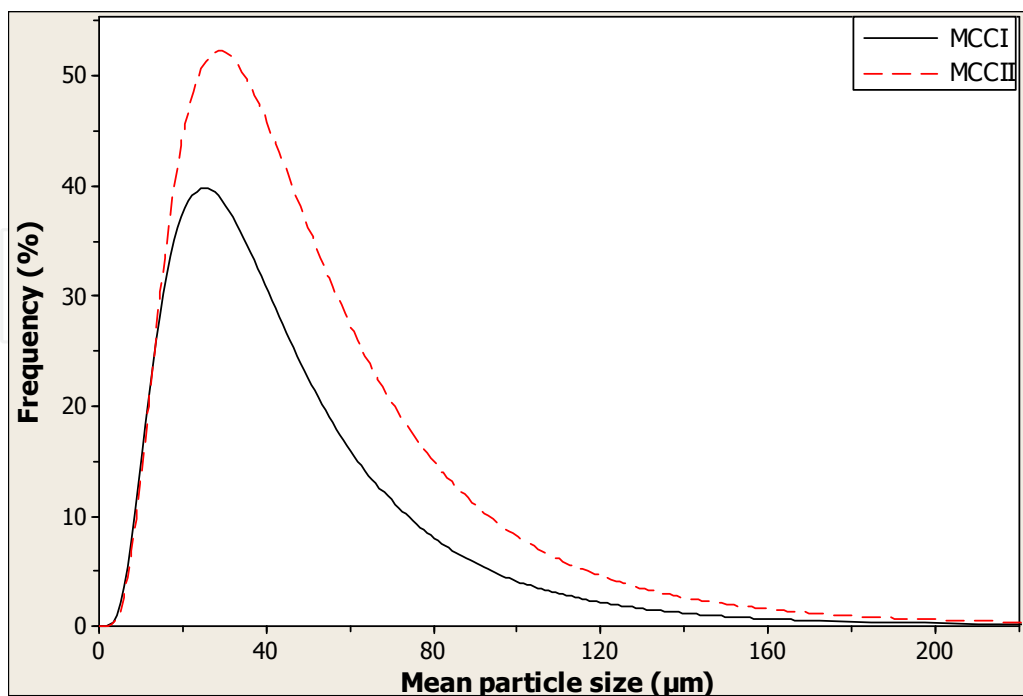**Figure 4.** Powder XRD of microcrystalline cellulose allomorphs

3.3. Powder properties

Figure 5 shows micrographs depicting particle morphologies. It seems to be that the polymorphic transformation had little effect on the morphology of these particles. Both, MCCI and MCCII consisted of aggregated and irregularly-shaped particles with rough surfaces and sharp edges. However, elongated particles were more predominant for MCCI. Table 1 lists the powder properties of these materials. Since the polymorphic transformation did not cause major morphological changes in the particles, the mean particle size of the two polymorphs was comparable. The particle size distribution is depicted in Figure 6. In this case, both materials showed a positively skewed distribution, but MCCII had a slightly larger tendency to have high frequencies in the low particle size region.

MCCI had a larger true density than MCCII. On the other hand, MCCII presented larger bulk and tap densities and consequently lower total powder porosity as compared to MCCI. The great ability of MCCII for particle packing could be due to morphological factors including its lower proportion of elongated particles, lower particle porosity and lower roughness. As a result, upon tapping or application of compression forces, MCCII is more likely to undergo a major volume reduction as indicated by its larger compressibility (52%). All these factors also contributed to an improvement in flow for MCCII. Thus, flowability was 3-fold larger for MCCII than for MCCI.

MCCI   MCCII

Figure 5. Optical micropictures of microcrystalline allomorphs

Figure 6. Particle size distribution of microcrystalline celluloses

The voluminosity of the powder was found by taking the reciprocal of the bulk density and thus, MCCII, due to its large packing ability, presented a lower voluminosity or bulkiness than MCCI.

The degree of polymerization (DP) is an indication of the average polymer length. The lower values of DP obtained for MCCII are probably due to the partial hydrolysis occurring during the NaOH treatment.

Property	n	MCCI	MCCII
Geometric mean (µm)	1	50.4 ± 7.4	56.5 ± 7.1
Compressibility (%)	1	33	52
Degree of polymerization	3	233.3 ± 0.6	183.6 ± 3.2
Molecular weight (g/mol)	1	37794.6	29743.2
Degree of crystallinity (%)	1	74.3	65.2
Porosity	3	0.78 ± 0.01	0.64 ± 0.01
Bulk density (g/cm³)	3	0.35 ± 0.01	0.55 ± 0.00
Tap density (g/cm³)	3	0.51 ± 0.00	0.76 ± 0.00
Voluminosity (ml/g)	3	2.9 ± 0.1	1.8 ± 0.0
True density (g/cm³)	3	1.578±0.05	1.540 ± 0.03
Flow rate (g/s)	3	1.61 ± 0.43	4.93 ± 0.96
Swelling value (ml/g)	3	0.2 ±0.1	0.8 ±0.0
Specific surface area (m²/g)	3	1.49 ± 0.05	0.53±0.05
Moisture content (%)	1	1.8	2.2

n=replicate

Table 1. Powder properties of microcrystalline celluloses

Figure 7 shows the isotherms curves fitted according to the Young-Nelson (YN) model and Table 2 shows the parameters derived from this model. All cellulosic materials exhibited a typical sigmoidal type II isotherm and the sorption and desorption curves showed hysteresis. Hysteresis is defined as the difference between the amount of water desorbed and sorbed. This difference creates a loop in the isotherm and is very common in hydrophilic materials. The amplitude of the loop is observed in Figure 7. This hysteresis was high between 0.2 and 0.7 water activities. Results indicate that hysteresis occurred throughout the sorption range and not just in the capillary condensation region as reported previously [33]. It is well known that the higher moisture content obtained when a polymer is desorbing from a saturated state is due to microcapillary deformation accompanied by the creation of more permanent hydrogen bonds which are no longer attainable in subsequent re-wetting processes. This phenomenon is known in cellulose as hornification [34].

Once cellulose sorbs water it swells slightly because microcapillaries expand due to the thermal motion of incoming water molecules forming new internal surfaces. Once water is removed, relaxation of the matrix to the original state is prevented. As a result, microcapillaries become greater on desorption compared to the adsorption step. In other

words, this hysteresis is caused by structural changes due to the disruption of the hydrogen bonding network of the polymer while interacting with water molecules. Therefore, the extra sorbed water showed by hysteresis is related to the structural or conformational changes of cellulose chains, which expose previously inaccessible high affinity sorption sites [35].

Since hysteresis took place mostly at a water activity of 0.2-0.7, it cannot be completely attributed to pore effects (ink bottle pores), but to swelling due to specific interactions of water sorbed in the bulk. The lower hysteresis of MCCI might indicate weaker specific interactions of its hydrophilic sites with water, and consequently, smaller structural reorganization of the chains due to cellulose swelling.

Figure 8 shows the deconvoluted curves for the monolayer and multilayer formation, respectively according to the YN model. It assumes that the monolayer and multilayers of water molecules are formed simultaneously at very low water activities. Furthermore, it considers the absorption of water into the core of particles to be the first step, followed by the layering process on the surface. MCCI showed the lowest fraction of water molecules that formed a monolayer and multilayer, respectively. Further, the amount of water absorbed in the core was considered as negligible. Thus, most of the cellulose water uptake can be attributed to adsorption due to layering.

The YN model also demonstrated that the fraction of water absorbed in the particles core was smaller than the fraction adsorbed as a monolayer and multilayer. Also, the H_1-H_L value for MCCII was very high, indicating the prevalence for layering formation, which is in line with the high hydrophilicity of this material. MCCII always showed higher affinity for water than MCCI as seen by the higher monolayer and multilayer formation at different water activities. This trend proved that the polymorphic transformation of MCCI into MCCII enhanced the water sorption capacity.
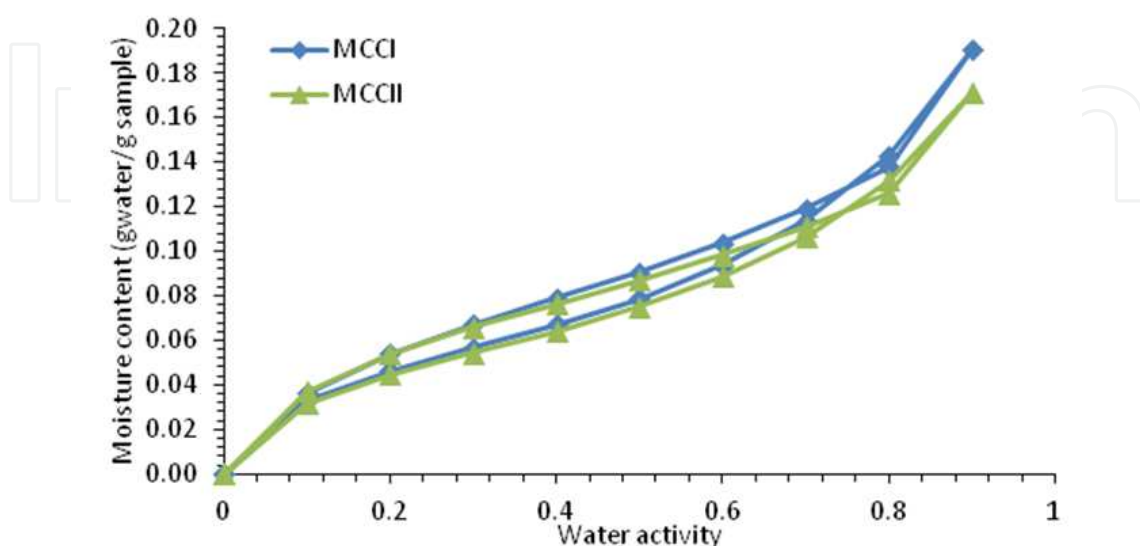
Figure 7. Water sorption and desorption isotherms according to the Young-Nelson model.
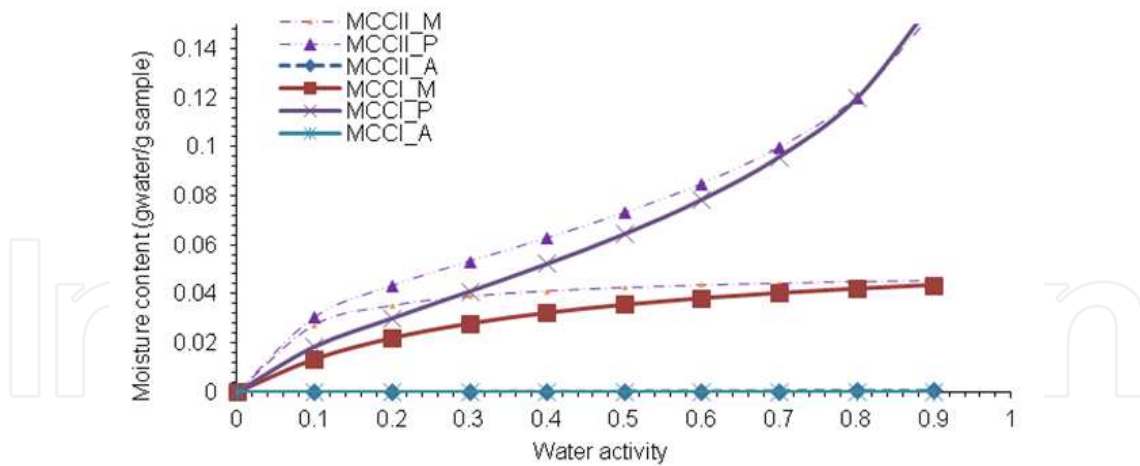
Figure 8. Deconvoluted Young-Nelson model for water sorption of microcrystalline celluloses. M, indicates monolayer formation, P, multilayer formation and A, the fraction attributed to the absorption process in the core of the particles.

In the YN model, the absorbed water has diffused through pores into the core of the particle from the adsorbed monolayer. The monolayer water is then the result of the balance between surface binding forces of the multilayer and water in the core. It is possible that water molecules bind as succeeding layers rather than to empty sites on the surface of the solid. Thus, the formation of a second layer probably starts at lower concentrations than those corresponding to the monolayer formation because the completion of the perfect monolayer would lead to a substantial decrease in entropy, which is very unlikely for natural polymers [36]. During the desorption phase vapor pressure is reduced and water molecules at the surface are removed before diffusion forces pull moisture out of the core of the material [37].

In the sorption phase, the curves of the monolayer formation presented a type I Langmuir isotherm, whereas the curves of the multilayer sorption showed a type II isotherm. The sorption of monolayer water is almost complete at a water activity of 0.1 for MCCII, whereas for MCCI it increased steadily up to 0.9 water activity. On the other hand, both polymers showed a constant increase of the multilayer formation throughout the whole water activity range. This proves that not all the adsorption sites of the first layer were filled when the formation of multilayers started. For this reason, the external moisture component isotherm had a type II shape and its contribution to the total amount of sorbed moisture increased with increasing water activities.

The parameters derived from the YN model are shown in Table 2. All samples had a good fit to the model ($r^2 > 0.9990$). The A (0.04-0.05) parameter confirmed that layering of water molecules either as a monolayer or multilayers was more prevalent than absorption into the core of the particles (B <0.01). Further, this absorption was more predominant for MCCII than for MCCI. The E and H_1-H_L values indicate that the formation of a monolayer for MCCII was energetically more favorable than the formation of multilayers. Further, H_1-H_L was positive, indicating the execution of an endothermic process. The E parameter was low

for MCCII indicating that the driving force for water sorption was higher than that of MCCI during the sorption phase. The first water molecule could bind to the 6-hydroxyl group because it is the most exposed hydroxyl group in cellulose [38]. Then, more incoming water molecules could bind to hydroxyl groups located in carbons 2 and 3 of the cellulose monomers.

Sample	A Mean ± SD	B Mean ± SD	E Mean ± SD	H_1-H_L kJ/mol	r^2
MCCI	0.04 ± 0.00	0.00 ± 0.00	0.26 ± 0.02	3.3	0.9990
MCCII	0.05 ± 0.01	0.01 ± 0.00	0.07 ± 0.05	7.4	0.9997

SD, standard deviation, A, fraction of adsorbed water; B, fraction of absorbed water;
E, equilibrium constant between the monolayer and liquid water; H_1-H_L, heat difference between absorption and condensation of water; r^2 coefficient of determination.

Table 2. Parameters obtained from the Young-Nelson model

The degree of crystallinity of MCCI was higher than that of MCCII. Therefore, as expected the less crystalline MCCII presented more water sorption sites due to its large amorphous component as compared to MCCI.

4. Compression studies

Although initially developed for metals, the Heckel analysis is widely used to assess the compressibility of pharmaceutical powders. Table 3 lists the Heckel analysis results. The yield pressure value, P_y, which is obtained from the inverse of the slope of the linear portion of the Heckel curve, refers to the pressure at which the material begins to deform plastically. A plastic deformation implies deformation and sliding of the crystals planes that consolidate the particles. Usually, a plastic deformation causes a minimum change in the surface area available for particle binding. On the other hand, brittle materials require extensive fragmentation for the formation of available surfaces for particle binding. In this case, large particles brake down into smaller particles upon compression. In general, the lower the P_y value, the higher the ductility of the material. In the present study, MCCI showed a low value, whereas MCCII exhibited a high P_y value (~93 MPa and 144 MPa, respectively). Therefore, MCCII is considered as less ductile than MCCI.

The D_0, D_a and D_b parameters, calculated from the Heckel plots, represent the initial packing of the material upon die filling, total packing at low pressures, and the degree of powder bed arrangement due to fragmentation at low pressures, respectively. The D_0 values follow the same trend than the bulk density values suggesting that the polymorphic transformation of MCCI into MCCII increased the ability of this material for packing. On the contrary, the total powder packing at low compression pressures remained unchanged. The D_b value as expected was higher for MCCI due to the less tendency to pack in the powder bed and thus, its particles were more able to rearrange at low compression forces.

Another widely used model for assessing compressibility of powders is the one proposed by Kawakita [17,18]. The "a" parameter indicates that MCCII was more compressible than MCCI. In other words, this material had a larger ability to reduce in volume upon compression. Likewise, the large "b" value for MCCII indicates that a tight packing arrangement in the powder bed generates a large resistant force for volume reduction. However, once consolidation starts, it is easier for MCCII to have a larger compressibility than MCCI.

5. Compactibility studies

Figure 9 shows the relationship between compact tensile strength and compression pressure. MCCI formed stronger compacts than MCCII. The magnitude of this difference appears to increase with increasing compression forces. The area under the curve of the tensile strength is an indication of the material compactibility. This compactibility was 4 times larger for MCCI than for MCCII suggesting this polymorphic transformation had a negative effect on the tensile strength of MCCI compacts. The small compact tensile strength values of MCCII are due to its low plastic deforming ability. These results indicate that the tight molecular arrangement of the chains and the higher plastic deforming ability of MCCI facilitate the formation of hydrogen bonding upon compression resulting in the formation of strong compacts.

Model	Parameter	MCCI	MCCII
Heckel	P_y (MPa)	92.6	144
	D_0	0.22	0.36
	D_a	0.48	0.45
	D_b	0.22	0.10
	r^2	0.9910	0.9850
Kawakita	A	0.33	0.52
	B	0.03	0.12
	r^2	0.9980	0.9999
Test	AUCTS	885.1	180.6
	Friability (%)	0.11	0.23
	SRS (%)	7.3	15.6
	D. Pot. (%)	24	20
	LSR	0.38	0.36

P_y, powder yield pressure; D_0, initial rearrangement as a result of die filling; D_a, total packing at low pressures; Particle rearrangement/fragmentation at early compression stages; a, Compressibility parameter; b, Indicates ease of compression; LSR, lubricant sensitivity ratio; SRS, strain rate sensitivity; D. Pot, dilution potential for acetaminophen; AUCTS, area under the tensile strength curve.

Table 3. Parameters obtained from the Heckel and Kawakita models and other tableting tests
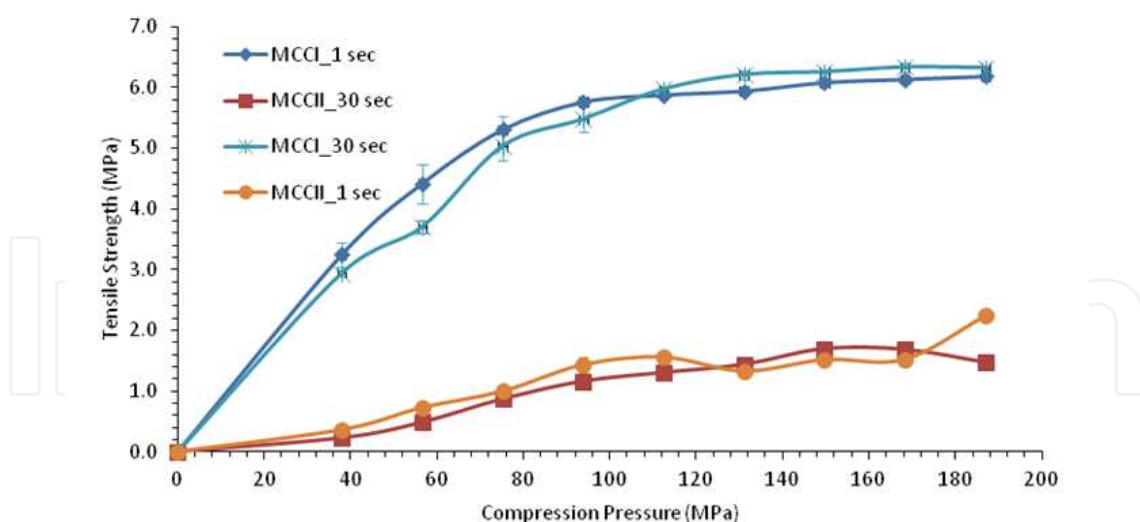
Figure 9. Compact tensile strength of the cellulose allomorphs

5.1. Dilution potential

To assess the effect of a poorly compressible substance on the compactibility of cellulose, compacts containing different weight ratios of the test material and acetaminophen were prepared and their crushing strength was determined. In this case, the crushing strength of the powder mixtures were plotted against the mass fraction of excipient and the resulting straight lines were interpolated to the X-axis to find the dilution potential. The dilution potential of MCCII (20%) was comparable to that of MCCI (24%). These results clearly suggest that MCCII and MCCI serve as effective binders and offer potential to produce tablets with poorly compressible drugs by direct compression. In fact, MCCI showed the highest compactibility but presented a comparable dilution potential for acetaminophen. This indicates that the presence of a poorly compressible drug affected the compactibility of MCCI much more than that of MCCII since a larger dilution potential was expected for MCCI.

5.2. Compact friability

Tablets prepared using 150 MPa compression pressures were tested for friability. All tablets had less than 1% friability indicating an optimum strength for handling and shipping. These results correlate well with the tensile strength results shown in Fig. 7. These findings clearly suggest that MCCI and MCCII serve as effective binders and offer potential to produce compacts with poorly compressible drugs by direct compression.

5.3. Lubricant sensitivity

Lubricant sensitivity was tested with magnesium stearate at a 1.0% w/w level in compacts made at 60 MPa of compression pressure. The presence of a surrounding layer of this hydrophobic lubricant had a large detrimental effect on MCCI since this material was the

most highly deforming material. Therefore, MCCI compactibility was reduced to a value comparable to that of MCCII. Moreover, the more fragmenting character of MCCII makes it able to create a large number of binding surfaces which counteract the coating effect exerted by magnesium stearate. In other words, magnesium stearate coats easily the surface of MCCI particles and thereby restricts the contact points between particles resulting in compacts of low strength. Thus, the lubricant film around particles in more fragmenting materials such as MCCII is not complete easing the formation of hard compacts.

5.4. Compact disintegration

Independent of compact porosity, compact disintegration time was less than 20 s for MCCII (Fig. 10). Only compacts of MCCI made at ~40 MPa passed the test requiring disintegration times of less than 30 min. The rapid disintegration times of MCCII are due to its larger swelling value and larger affinity for water as compared to MCCI. Further, it is possible that the low degree of crystallinity of MCCII played an important role in its rapid disintegration. The effect of compact porosity was considered as negligible since all compacts were made at 10-20% porosity. These results indicate that when MCCI is employed as excipient for making tablets, it always requires the addition of a superdisintegrant, which is a material with a large affinity for water that enhances compact disintegration. On the contrary, MCCII does not require that ingredient due to its intrinsic disintegrating properties.
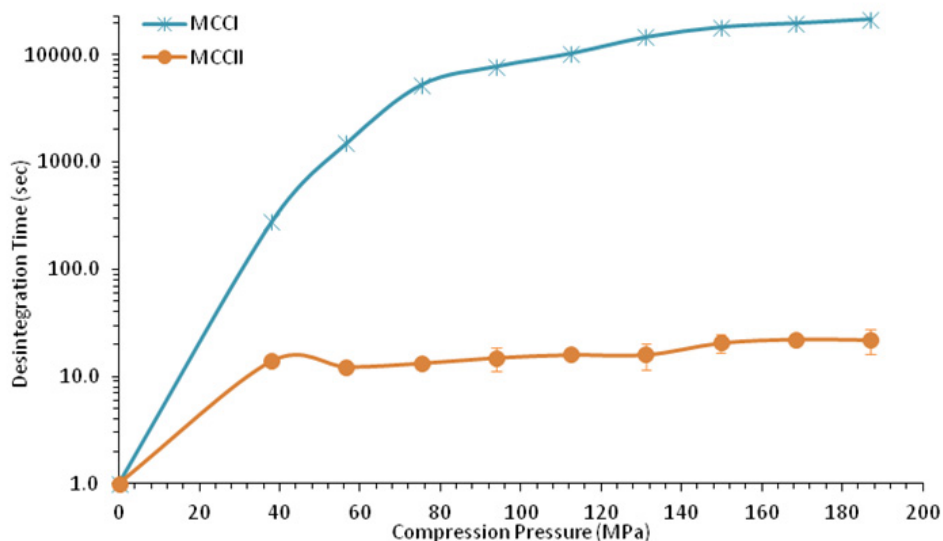
Figure 10. Compact disintegration time of the cellulosic materials.

6. Conclusions

The polymorphic transformation had a major effect on the degree of polymerization, degree of crystallinity, packing tendency, bulk and tap densities, voluminosity, swelling ability and water sorption rate of microcrystalline cellulose. MCCII exhibited a faster disintegration ability, but lower compactibility than MCCI due to its large amorphous component. However, when MCCII was mixed and compressed with acetaminophen it was as

compactable as MCCI and possessed a comparable acetaminophen loading capacity and lubricant sensitivity as those of MCCI.

Particle morphology and particle size were not affected, but compact tensile strength was highly affected by the polymorphic transformation. Most of the resulting particle and tableting properties depended on the polymorphic form of MCC. For this reason, it is important to select the right crystalline form of MCC before formulating a drug in a solid dosage form since it could affect the overall particle and tableting properties of the mixture.

Cellulosic excipients are hydrophilic materials and the polymorphic transformation caused differences in the hydrophilic properties of cellulose. Most of the water sorption isotherms exhibited a type II sigmoid shape and MCCII presented the largest water uptake by absorption into the core of the particles.

Cellulosic materials showed a hysteresis loops which were caused by capillary shrinking during the desorption step. The YN model assume sorption and desorption as a dynamic process, in which the primary sorption sites are filled up throughout the whole water activity range and do not require the formation of a complete monolayer to form a multilayer.

Author details

John Rojas
Department of Pharmacy, School of Pharmaceutical Chemistry, The University of Antioquia;
Medellín, Colombia

Acknowledgement

7. References

[1]   Klemm D, Philipp B, Heinze T, Heinze U (1998a). Comprehensive Cellulose Chemistry: Functionalization of Cellulose. New York, USA: John Wiley. 389 p.

[2]   Klemm D, Philipp T, Heinze U, Wagenknecht W, editors (1998b). Comprehensive Cellulose Chemistry: Fundamental and Analytical Methods. John Willey. pp.107-249.

[3]   Krassig H (1996). Cellulose, Structure, Accessibility and Reactivity. Gordon and Breach Science Publishers, Amsterdam, Holland. 376 p.

[4]   Kroon-Batenburg LMJ & Kroon J (1997). The crystal and molecular structure of cellulose I and II. *Glycocon J.* 14: 677-690.

[5]   Blackwell J & Kolpak FJ (1975). The Structure of Regenerated Cellulose. *Macromolecules,* 8: 563-564.

[6]   Battista O (1965). Colloidal macromolecular phenomena. *J Polym Sci Pol Sym.* 9:135-155.

[7]   Kolpak FJ & Blackwell, J (1976). Determination of the structure of cellulose II. *Macromolecules* 9, 273-278.

[8]   Battista O & Smith P (1961). Level-off degree of polymerization cellulose products. US Patent No. 2978446.

[9]   Lerk C & Vromans H (1988). Densification properties and compactibility of mixtures of pharmaceutical excipients with and without magnesium stearate. *Int J Pharm.* 46: 183–192.

[10] Moreton R (1996). Tablet excipients to the year 2001: A look into the crystal ball. *Drug Dev Ind Pharm*. 22:11-23.

[11] Westermarck S, Juppo AM, Kervinen L, Yliruusi J (1999). Microcrystalline cellulose and its microstructure in pharmaceutical processing. *Eur J Pharm Biopharm*. 48:199-206.

[12] Kumar V, Reus M, Yang D (2002). Preparation, characterization, and tableting properties of a new cellulose-based pharmaceutical aid. *Int J Pharm.* 235: 129–140.

[13] Kumar V & Reus M (2006). Evaluation of cellulose II powders as a potential multifunctional excipient. *Int J Pharm.* 322: 31–35

[14] Rojas J & Kumar V 2012. Effect of polymorphic form on the functional properties of cellulose: A comparative study. *Carbohyd Polym.* 87: 2223-2230.

[15] Rabek JF 1980. Experimental Methods in Polymer Chemistry. Bristol, UK: John Wiley. 861 p.

[16] Meyer V, editor (2006). Annual Book of American Society of Testing and Materials. Section 6. Paints Related Coatings and Aromatics. West Conshhocken, PA: ASTM International. 403 p.

[17] Kawakita K & Ludde KH (1971). Some considerations on powder compression equations. *Adv Powder Tech.* 4: 61-68.

[18] Yamashiro M, Yuasa Y, Kawakita K (1983). An experimental study on the relationships between compressibility, fluidity and cohesion of powder solids at small tapping numbers. *Powder Technol*. 34:225-231.

[19] Edge S, Steele DF, Staniforth JN, Chen A, Woodcock P (2002a). Powder compaction properties of sodium starch glycolate disintegrants. *Drug Dev Ind Pharm*. 28: 989-999.

[20] Young JH & Nelson GH (1967). Theory of hysteresis between sorption and desorption isotherms in biological materials. *Trans Am. Soc. Agric. Eng*. 10: 260-263.

[21] Nokhodchi A, Ford JL, Rubinstein HL (1997). Studies on the interaction between water and (hydroxypropyl) methyl cellulose. *J Pharm Sci*. 86: 608-615.

[22] Heckel RW (1961a). An analysis of powder compaction phenomena. *Trans Metal Sci AIME* 221:1001-1008.

[23] Heckel RW (1961b). Density-pressure relationship in powder compaction. *Trans Metal Sci AIME* 221:671-675.

[24] Alderborn G & Nyström C (1996). Pharmaceutical powder compaction technology. New York: Marcel Dekker Inc. 615p.

[25] York P (1992). Crystal engineering and particle design for the powder compaction process. *Drug Dev Ind Pharm* 18: 677-721.

[26] Chow YP & Chowhan CT (1980). Compression behavior of pharmaceutical powders. *Int J Pharm.* 5: 139-148.

[27] Fell JT & Newton JM (1968) The tensile strength of lactose tablets. *J Pharm Pharmacol*. 20: 657-758.

[28] Carrillo F, Colom X, Saurina J, Sunol J (2004). Structural FTIR analysis and thermal characterization of lyocel and viscose-type fibers. *Eur Polym J*. 40: 229- 234.

[29] Zhbankov RH (1966). Infrared spectra of cellulose and its derivatives. New York: Consultants Bureau, 333 p.

[30] Iida K, Aoki K, Danjo K, Otsuka A, Chen CY (1997). A comparative evaluation of the mechanical properties of various celluloses. *Chem Pharm Bull*. 45: 217-220.

[31] Suzuki T & Nakagami H (1999). Effect of microcrystalline cellulose on the compactibility and dissolution of tablets. *Eur J Pharm Biopharm*. 47: 225-230.

[32] Kothari SH, Kumar V, Banker GS (2002). Comparative evaluation of powder and mechanical properties of low crystallinity celluloses, microcrystalline celluloses, and powdered celluloses. Int J Pharm. 232:69-80.

[33] Parker ME, Bronlund JE, Mawson AJ (2006). Moisture sorption isotherms for paper and paperboard in food chain conditions. *Packag Technol Sci*.19: 193-209.

[34] Pizzi A, Eaton NJ, Barista M (1987). Theoretical water sorption energies by conformational analysis. *Wood Sci Technol*. 2: 235-48.

[35] Kmetes V & Koskar R (2005). Evaluation of the moisture sorption of several excipients by BET, GAB and microcalorimetric approaches. *Chem Pharm Bull*. 53: 662-665.

[36] Khan F & Pipel N (1986). Water solid interactions II. Effect of moisture sorption and glass transition temperature on compactibility of microcrystalline cellulose alone or in binary mixtures with polyvinyl pyrrolidone *Powder Tecnol*. 48: 145-50.

[37] Kochervitov V, Ulvenlund S, Kober M, Jarring K, Arnebrant T (2008). Hydration of microcrystalline cellulose and milled cellulose studied by sorption calorimetry, J Phys Chem B. 112: 3728-3734.

[38] Hartley DI, Kamke FA, Peemoeller H (1992). Cluster theory for water sorption in wood *Wood Sci Technol*. 26: 83-99.